5-2015

Coupling Soil Oxygen and Greenhouse Gas Dynamics

Karla M. Jarecke
University of Nebraska-Lincoln, jareckek@gmail.com

COUPLING SOIL OXYGEN AND GREENHOUSE GAS DYNAMICS

by

Karla M. Jarecke

A THESIS

Presented to the Faculty of

The Graduate College at the University of Nebraska

In Partial Fulfillment of Requirements

For the Degree of Master of Science

Major: Natural Resource Sciences

Under the Supervision of Professor Amy J. Burgin and Terrence D. Loecke

Lincoln, Nebraska

May, 2015

COUPLING SOIL OXYGEN AND GREENHOUSE GAS DYNAMICS

Karla M. Jarecke, M.S.

University of Nebraska, 2015

Advisers: Amy J. Burgin and Terrence D. Loecke

Dynamic soil hydrology triggers important shifts in soil biogeochemical and physical processes that control greenhouse gas (GHG) emissions. Soil oxygen (O_2), a direct control on biogenic GHG production (e.g. nitrous oxide-N_2O, carbon dioxide-CO_2 and methane-CH_4), may serve as both an important proxy for determining sudden shifts in subsurface biogenic GHG production as well as the physical transport of soil GHG to the atmosphere. Recent technological advancements offer opportunities to link *in-situ*, near-continuous measurements of soil O_2 concentration to soil biogeochemical processes and soil gas transport. Using high frequency data, this study asked: Do soil O_2 dynamics correspond to soil GHG concentration and GHG surface flux? Change in subsurface CO_2 and N_2O concentrations were inversely related to short-term (< 48 hrs) change in soil O_2 concentration at 10 and 20 cm whereas CH_4 concentrations did not change in response to soil O_2 dynamics. Although soil O_2 dynamics at 10 cm did not correspond with change in surface N_2O and CH_4 flux, change soil O_2 concentration at 10 cm had a significant positive linear relationship with change in surface CO_2 flux. Our study suggests that coupling near-continuous soil O_2 concentration and soil gas flux under dynamic soil hydrology may lead to greater understanding of climate change feedbacks and serve as a relevant predictive tool for future climate change mitigation.

Acknowledgements

I thank Astrea Taylor, Cain Silvey, Dave Moscicki, Joanna Taylor, Carrie Adkisson, and Monica Christian for their help with field and laboratory analyses. Fondriest Environmental and Stevens Water provided helpful technical support with the sensor network. We also acknowledge Fiver Rivers Metro Parks for allowing us to complete this research on the Great Miami Mitigation Bank. This project was funded by NASA/USDA joint program on Carbon Cycle Science (awards 2011-03007 and 2011-00829).

Table of Contents

LIST OF MULTIMEDIA OBJECTS

Introduction

Brief periods of disproportionately high rates of soil-atmospheric biogenic GHG (carbon dioxide, CO_2, nitrous oxide, N_2O and methane, CH_4) exchange, known as "hot moments", contribute significantly to whole-system GHG budgets (Groffman et al. 2009, Vargas et al. 2010). Hot moments in GHG emission are often triggered during transitional periods in soil hydrology (e.g., soil re-wetting and thawing) that induce sudden change in the biological and physical soil environment (Kim et al. 2012, Malodovskaya et al. 2012). Although hot moments may significantly alter estimates of nutrient fluxes (McClain et al. 2003), the biogeochemical and physical mechanisms that drive spatiotemporal variability in GHG emissions from dynamic landscapes are poorly understood (Groffman et al., 2009). Therefore, accurately predicting the occurrence of hot moments and quantifying their magnitude is increasingly important for estimating positive feedbacks to climate change. This will require more precise descriptions of the environmental drivers of CO_2, CH_4, and N_2O production/consumption as well as GHG transport during soil re-wetting and drying (Blagodatsky et al. 2012, Chen et al., Fumoto et al. 2008, Riley et al. 2011).

An important, but understudied, driver of soil GHG fluxes is soil O_2 availability. Soil O_2, by its control on redox potential, is an important control on aerobic and anaerobic biogeochemical processes and subsequent GHG production and consumption (Burgin et al. 2011, Silver et al. 2012). In lieu of rare direct measurements, scientists commonly assume soil O_2 availability from soil water content (Heinen et al. 2006). However, measuring soil O_2 dynamics may be useful to explore mechanisms of

biogeochemical shifts (Liptzen et al. 2011). The studies that have measured soil O_2, find concentrations to be dynamic on short temporal scales (hours to weeks) under varying hydrological conditions as a result of seasonal water table or precipitation patterns (Burgin and Groffman 2012, Hall et al. 2013, Liptzen et al. 2011, Silver et al. 1999, Teh et al. 2005, Loecke et al. [in review]). In mineral soils, the rate of soil O_2 depletion under saturation depends on temperature (Loecke et al. [in review]), which suggests a strong connection of soil O_2 availability to increased microbial respiration that is commonly observed under increased temperature and labile substrate supply (Fierer and Schimel 2003). Dry soils, in contrast, limit biological activity under low solute diffusion and water stress (Harris 1981), but permit the rapid diffusion of atmospheric O_2 to the soil. Loecke et al. refer to the quick re-supply of atmospheric O_2 to the soil that occurs on an hourly timescale during soil drying as the "big gulp". Big gulps indicate sudden shifts in soil gas diffusivity that may permit a directionally opposite transport of soil gases to the atmosphere (Loecke et al. [in review]). However, studies that measure soil O_2 concentrations have yet to understand how the timing of soil O_2 fluctuation corresponds to soil-atmospheric GHG fluxes.

Given the important role of soil O_2 availability on biogeochemical processing, our goal is to assess soil O_2 as a biogeochemical driver of GHG production/consumption as well as a physical indicator of soil GHG transport. Short-term soil O_2 fluctuations under varying hydrology may be a useful proxy for understanding the timing of briefly enhanced rates of surface GHG fluxes (hot moments). With the use of high frequency soil O_2 and soil moisture sensors, this study addresses how soil GHG concentrations and

surface GHG fluxes correspond to near-surface (10 and 20 cm depth) soil O_2 dynamics. During sustained soil saturation, we expected the depletion of soil O_2 present in water-filled pore space and restrictive diffusion of soil GHGs to the atmosphere to result in an increase in subsurface GHG concentrations at 10 and 20 cm and a decrease in GHG surface fluxes. During soil drainage, we expected the rapid influx of atmospheric O_2 ("big gulp") to co-occur with a decrease in subsurface GHG concentrations and an increase in surface GHG fluxes permitted by rapid soil gas diffusion in air-filled pore space. We discuss how further examination of soil O_2 dynamics may improve our ability to model spatiotemporal variability of GHG emissions and understand the importance of hot moments in a changing climate.

Materials and Methods

Study Site

Our research is conducted at the Great Miami Wetland Mitigation Bank, a 46 ha restored wetland in Trotwood, Montgomery County, Ohio, United States (36°46'51" N, 84°20'26" W). Five Rivers Metro Parks, Dayton, OH funded and managed the restoration project, which serves as a wetland mitigation bank. The bank was formed to provide compensatory mitigation for impacted waters of the United States, including wetlands and streams, which result from activities authorized under the Clean Water Act (NRC, 2001). The restoration involved extensive earth moving during 2011 and planting native wetland and upland vegetation during 2012. The site, previously drained for row crop production for over 100 years, is underlain by poorly drained silty clay loam (Brookston, Fine-loamy, mixed, active, mesic Aeric Endoaqualfs). Average annual regional

precipitation is 1005 mm and average annual temperature is 10.8˚C. Average daily temperature during our study was 11.93 ˚C in October 2013 and 21.37˚C from June-August 2014. The site received a total 147 mm of rain in October 2013 and approximately 178 mm from June to August 2014.

We installed soil sensors and gas sampling chambers at two sites approximately 200 m apart. We chose the location of the sites to represent differences in soil texture across the restored wetland (Figure 1a and Table 1). Soil texture at 0-10 cm across the restored wetland was estimated from 120 soil cores collected post-construction in November 2011. The soil at the quick draining (QD) site is sandy clay loam soil at 0-10 and 10-20 cm, which had shorter saturation duration following precipitation events in 2014 compared to the slow draining (SD) site with clay soil (0-10 cm) and clay loam soil (10-20 cm) (Table 1). In September 2013, we installed the QD site with five replicated sampling pits positioned approximately two meters from the nearest neighboring pit. In May 2014, we added the SD site with three replicated sampling pits positioned approximately two meters apart. QD is located in an area where intensive earth moving occurred (2010-2011); SD experienced minimal impact under construction activity.

Sensor and Gas Chamber Installation

Data loggers at each site (Campbell Scientific CR1000, Nexens 3100-iSIC, and Stevens DOT) recorded hourly soil O_2, soil moisture and soil temperature. We sampled GHG subsurface concentrations and GHG surface flux during October 2013 at QD and from June to August 2014 at QD and SD. Each pit consisted of two SO-110 soil O_2 (Apogee Instruments, Logan, Utah), two SDI-12 hydra probe (Stevens Water, Portland,

Oregon), and four subsurface gas chambers installed horizontally 15-20 cm from a neighboring sensor at 10 and 20 cm depth (Figure 1b). Soil O_2 sensors were secured vertically to a 30.5 cm diffusion head made of perforated polyvinyl chloride (PVC) pipe (1.9 cm ID, 2.54 cm OD). Subsurface gas chambers were constructed with 30.5 cm of silicone tubing (1.27 cm ID, 0.32 wall thickness) secured in perforated PVC pipe (1.9 cm ID, 2.54 cm OD) and fit to a tygon lead that ran to the surface for sampling with a stopcock and syringe. The average time to 95% equilibration with surrounding CO_2 concentration is 9.1 hours for silicone tubing with wall thickness equal to 0.32 cm (DeSutter et al. 2006). Prior to installing soil O_2 diffusion heads and subsurface gas chambers, we drilled a hole of slightly smaller diameter into the soil wall with a 1.9 cm auger bit. Above each sampling pit, we placed static surface flux chambers (12.5 cm in length x 25 cm inside diameter) outfitted with a PVC lid with a small sampling port needle vent to permit equilibration of internal and external atmospheric pressure (modified from Robertson et al., 1999). We positioned the center of the permanent collars 30 cm from the pit wall to ensure surface gas fluxes were collected directly above subsurface sensors and gas chambers. Surface gas chamber collars were inserted 3-5 cm into the soil. We saw no visible evidence of cracking at the soil surface and allowed chambers to settle two weeks prior to sampling.

Soil Analyses and Gas sampling

In June 2014 we collected three replicated 30 cm soil cores at QD and SD one meter from the surface flux chamber where soils were undisturbed during sensor installation. We cut cores in 2 sections: 0-10 cm and 10-20 cm. We assessed each section

for soil physical properties including bulk density, percent sand, percent silt, percent clay, total carbon, total nitrogen, and substrate-induced respiration (West, 1986). The two sites are significantly different ($\alpha = 0.05$) in bulk density, texture characteristics, substrate induced respiration (SIR), and total nitrogen, but do not differ in total carbon (Table 1). Average SIR at 0-10 cm was 5 times greater at SD compared to QD soil at 0-10 cm; average SIR at SD near-surface soil (0-10 cm) was also five times greater than deeper soil (10-20 cm) whereas SIR did not differ between depths at QD (Table 1).

In total, we sampled subsurface soil gas and surface gas flux 20 times at QD during October 2013, 54 times at QD from June to August 2014, and 56 times at SD from June to August 2014. We collected subsurface and surface gas samples 1-2 times prior to precipitation and twice daily immediately following precipitation until soil O_2 returned to stable, near-atmospheric concentration at all locations. In August 2014, we used supplemental irrigation to mimic rainfall by pumping water from an artesian well approximately 400 meters to an elevated, rotating sprinkler that distributed water equally at each pit.

Subsurface gas samples were collected into a 6 mL Exetainer (Labco, Exeter UK) vial previously flushed with N_2 and consisted of 3 mL of chamber soil gas after flushing 1.5 mL from the lead tubing. Immediately following subsurface soil gas collection, we collected gas samples (10 mL) from soil surface chamber headspace with a stopcock and syringe at 0, 15, 30, and 45 minute time points and transferred into a 6 mL Exetainer vial with atmospheric background. All gas samples were immediately shipped to the University of Nebraska-Lincoln and analyzed on an Agilent gas chromatograph (GC)

using flame ionized detector (FID) for CH_4, electron capture detector (ECD) for N_2O, and external CO_2 analyzer (LICOR 820). For QA/QC, we analyzed one check sample of known CO_2, N_2O, and CH_4 concentration for every twenty field samples; if the coefficient of variation for checks was less than 3% we accepted GC results that fell within the detection limits of our standard curve.

Data Analysis: Characterizing Soil O_2 and Saturation Events

Rapid increases in soil O_2 or big gulps were characterized by positive change in sequential measurements of soil O_2 concentration that exceeds 1.2%. This change in soil O_2 concentration also occurred twice within 5 hours to ignore fluctuations in soil O_2 concentration due to diurnal change and sporadic noise in soil O_2 measurements. We quantified the local minimum and maximum soil O_2 concentration within 20 hours before and after the big gulp to understand the magnitude of soil O_2 loss. To understand how saturation duration influenced soil O_2 loss, we quantified soil saturation using local threshold values for soil moisture (cm^3 cm^{-3}). We defined local saturation thresholds by subtracting 0.04 from the 99th percentile of measured soil moisture to remove measurement noise. The start of the saturation event occurred when soil moisture measured above the threshold 4 times in 2 hours; the end of the saturation event occurred when soil moisture measured below the saturation threshold 4 times in 2 hours. These criteria ignored short-term (< 2 hours) increases in soil moisture that did not induce change in soil O_2 concentration. We used the time at the start and end of the saturation event to calculate the total time soil remained saturated (saturation duration) at each

location. We analyzed the response of soil O_2 loss to saturation duration at QD and SD 10 and 20 cm using linear regression models ($\alpha < 0.05$).

We collected GHG samples during saturation and within 24 hours of the big gulp at QD 10 cm (n=16), QD 20 cm (n=8), SD 10 cm (n=13), and SD 20 cm (n=10). We determined the percent of these events in which CO_2, N_2O, and CH_4 concentrations at 10 and 20 cm decreased following the big gulp by subtracting the maximum concentration during saturation (start of saturation to big gulp) from the maximum concentration within 24 hours following the big gulp. We repeated this analysis for CO_2, N_2O, and CH_4 surface fluxes to determine the percent of events in which surface flux increased following the big gulp.

Finally, to understand the effect of dynamic soil O_2 on measured GHG concentrations and surface fluxes, we estimated: 1) Change in subsequent GHG concentration and surface GHG flux for samples collected within 48 hours and 2) Simultaneous change in soil O_2 concentration. We analyzed the linear and quadratic response of change in subsurface GHG concentration (10 and 20 cm) and surface GHG flux to simultaneous change in soil O_2 concentration when change in soil O_2 was greater than 3%; 3% represents more than two times the average diurnal change in soil O_2 concentration. All data analysis was performed in R© (R Core Team, 2014).

Results

During June-August 2014, soil moisture ranged from 0.1 to 0.6 cm^{-3} cm^{-3}; soil O_2 concentration ranged from 1.3 to 21% among QD and SD sampling locations. Following precipitation events in October 2013 and June-August 2014, we observed two repeated

patterns in soil O_2 dynamics: 1) Soil O_2 declined as a lagged response to soil moisture increase (Figure 2b solid arrow) and 2) Soil O_2 increased rapidly (defined as "the big gulp" in Loecke et al. [in review]) during soil drainage (Figure 2b dashed arrow). Soil O_2 loss was spatially variable across 10 and 20 cm sampling locations following June-August 2014 precipitation (Figure 3a-d). On average, SD (slow draining) had greater loss in soil O_2 concentration (%) and longer periods of saturation compared to QD (quick draining) at both 10 and 20 cm (Table 1). At least two occasions of soil O_2 loss greater than 1.2% occurred across sampling locations with the exception of QD "r5" at 20 cm depth (Figure 3). Overall, soil O_2 depletion followed by the big gulp occurred more frequently at 10 cm than 20 cm (Table 1). Soil O_2 loss across all site and depth combinations was a positive linear function of saturation duration ($p<0.001$; $R^2=0.30$). Soil O_2 loss increased significantly with duration saturated at QD 10 cm ($p= 0.01$; $R^2 = 0.25$; Figure 4a), SD 10 cm ($p=0.01$; $R^2 = 0.34$; Figure 4a), and SD 20 cm ($p< 0.001$; $R^2 = 0.75$; Figure 4b). Soil O_2 loss at QD 20 cm had the strongest positive relationship with saturation duration ($R^2 = 0.75$), whereas, the linear response of soil O_2 loss to saturation duration at QD 20 cm was not significant (Figure 4b).

Figure 5 contrasts the response of soil moisture and soil O_2 following June precipitation at QD and SD. At QD soil O_2 remained relatively stable at 10 and 20 cm during soil saturation following quick drainage, as indicated by decreased soil moisture. Simultaneously, CO_2 concentration increases, but N_2O and CH_4 concentration remain relatively unchanged (Figure 5a,c). In contrast, soil O_2 loss was greater at SD under sustained saturation and increases in soil CO_2, N_2O, and CH_4 concentrations were also

greater (Figure 5b,d). Surface CO_2 flux was dynamic at both QD (Figure 6a) and SD (Figure 6b) for sampling locations represented in Figure 5. Although CO_2 surface flux was dynamic at both sites, N_2O surface flux increased more at SD compared to QD whereas CH_4 decreased slightly from pre-saturation conditions at both sites (Figure 6a,b).

We predicted that GHG concentration would decrease following big gulps due to the increased diffusion of soil gases under soil drainage. Overall, we observed this pattern most often with N_2O. Decreased N_2O concentration following the big gulp occurred more often at SD (100 % decreasing events at 10 cm and 85% decreasing events at 20 cm) compared to QD. CO_2 concentration also decreased more often at SD compared to QD with the greatest number of decreasing events (90%) occurring at SD 20 cm (Table 2); CH_4 concentration decreased less frequently overall with the greater number of decreasing events (69%) at SD 10 cm (Table 2). We predicted that increased soil gas diffusion during soil drainage and subsequent big gulps would also result in increased surface GHG fluxes. Surface CO_2 flux increased most often following big gulps at 10 cm (63% at QD and 85% at SD) whereas surface N_2O flux increased for only 13% of big gulp events at QD and 54% at SD; CH_4 flux increased for approximately one-third of big gulp events (31% at QD and 38% at SD) (Table 2).

Change in CO_2 surface flux had a positive linear relationship with change in soil O_2 concentration at 10 cm (Figure 7a). We observed increased surface CO_2 flux during increased soil O_2 concentration at 10 cm and decreased surface CO_2 flux during decreased soil O_2 concentration. Change in N_2O and CH_4 surface fluxes were not significantly related to change in soil O_2 concentration at 10 cm (Figure 7b,c). The

change in CO_2 and subsurface concentration at 10 and 20 cm was inversely related to the change in soil O_2 concentration (Figure 7d $p<0.001$; $R^2=0.58$ at 10 cm and $p<0.001$, $R^2=0.35$ at 20 cm). Change in N_2O concentration was also inversely related to change in soil O_2 at 20 cm (Figure 7e $p=0.003$; $R^2=0.24$). However, N_2O concentration at 10 cm was a quadratic function of soil O_2 change (Figure 7e $p=0.03$; $R^2=0.14$) with exponential increase in N_2O concentration occurring during soil O_2 decrease. CH_4 concentration did not significantly respond to soil O_2 dynamics at 10 cm or 20 cm (Figure 7f).

Discussion

Our challenge was to understand if soil O_2 availability corresponds to shifts in subsurface GHG concentrations and surface GHG fluxes. We found that the magnitude of soil O_2 loss following short-term (hours to days) saturation varies horizontally and with soil depth (10 and 20 cm) and is predicted by duration of soil saturation. We detected significant increase in subsurface CO_2 and N_2O concentration in response to slow soil gas diffusion and soil O_2 depletion. We also determined that rapid soil O_2 increase corresponds with a decrease in subsurface CO_2 and N_2O concentration and an increase in surface CO_2 flux. We will examine the effect of soil O_2 dynamics on biogenic GHG in greater detail below and explore the implications of soil O_2 dynamics for understanding biogeochemical hot spots and hot moments.

Soil O_2 effects on biogenic greenhouse gases

Subsurface CO_2 concentration dynamics are inversely related to soil O_2 dynamics following soil wetting and drying (Figure 7d,e). CO_2 concentration dynamics had the strongest relationship with soil O_2 dynamics, which suggests that soil O_2 availability

under short-term soil saturation creates conditions for carbon mineralization under increase labile substrate. Several studies report enhanced CO_2 flux during soil re-wetting (Harris 1981, Fierer & Schimel 2002, Ryals & Silver 2013), but the subsequent decrease in soil CO_2 concentration that we observed co-occurs with big gulps (Figure 7d) initiated by soil drainage. In addition, big gulps correspond to increase CO_2 surface flux and soil O_2 loss corresponds with decreased CO_2 surface flux. This link between short-term, dynamic soil O_2 and CO_2 concentrations as well as near-surface soil O_2 concentration and CO_2 surface flux has not been reported by other studies. Furthermore, the greatest change in CO_2 concentrations and CO_2 surface flux occurred at SD where magnitude of soil O_2 loss and subsequent big gulps were greater (Figure 7a,d). Thus, we conclude that greater magnitude of soil O_2 loss triggers greater shifts in short-term (< 48 hrs) CO_2 concentration and surface CO_2 flux.

Unlike CO_2, a terminal product of heterotrophic oxidation of organic matter, N_2O is readily produced and consumed in soil (N_2O reduction to N_2). N_2O is generally controlled by dynamic production and consumption processes—nitrification and denitrification (Burgin et al. 2010). Although production of N_2O often exceed consumption rates, N_2O can be further reduced to N_2 (via denitrification) under diffusional constraints in the soil profile by infiltrating water (Clough et al. 2005) . Similar to CO_2 concentration, change in soil N_2O concentration had an inverse linear relationship with simultaneous change in soil O_2 at 20 cm; at 10 cm, change in soil N_2O concentration had a negative quadratic relationship with change in soil O_2. Greater soil O_2 loss resulted in greater increase in N_2O concentration at SD compared to QD (Figure

7e). Furthermore, the greatest increases in N_2O concentration occurred when soil O_2 loss exceeded 5%. Liptzen et al. also measure high N_2O concentrations at near-atmospheric soil O_2 concentration in tropical soils. Thus, the increase N_2O concentration that occurred in a relatively oxic soil profile may be a result of nitrification or denitrification in anoxic microsites.

Consistently inundated soils that limit O_2 availability can increase CH_4 production from methanotrophic bacteria and favor CH_4 transport via plants or ebullition (Whalen 2005). The short-term saturation events that occurred in this study can stimulate both CH_4 production and oxidation and lead to lower CH_4 surface flux in dynamic systems (Altor & Mitsch 2008, van Bodegom et al. 2000). Soil CH_4 concentration can have a strong negative non-linear relationship with soil O_2 concentration when soil O_2 concentration is extremely low (<1%) for extended periods (months) in wet tropical soils (Liptzin et al. 2011). In our study, average soil O_2 loss following precipitation ranged from 4.3 to 6.6% (Table 1) and we find change in CH_4 concentration in the bulk soil was unaffected by short-term soil O_2 dynamics (Figure 7f). The CH_4 produced in anoxic microsites in saturated soil was likely quickly oxidized before reaching the soil surface. If QD and SD receive more frequent or longer periods of precipitation, extended water infiltration or water table rise may lead to prolonged periods of low soil O_2 and greater soil CH_4 concentrations under restricted diffusion.

Using soil O_2 to understand biogeochemical hot spots and hot moments

Spatial and temporal variation in near-surface soil O_2 dynamics may be useful for understanding the presence (hot spots) and timing (hot moments) of disproportionately

high GHG surface fluxes. The spatial heterogeneity in soil O_2 loss that we observed between and within SD and QD may be strongly linked to soil drainage patterns influenced by site-specific soil physical properties (i.e., soil texture) and topography. In addition to soil hydrologic properties, the spatial differences in soil O_2 loss may reflect heterogeneity in microbial O_2 demand (Rubol et al. 2013). An increase in microbial O_2 demand under prolonged soil saturation would support our observations of greater increases in CO_2 and N_2O concentrations at SD during greater soil O_2 losses. Furthermore, SD soil had significantly higher substrate induced respiration rates at 0-10 cm compared to QD (Table 1). Our results support that both hydrologic properties and microbial O_2 demand are important drivers of subsurface GHG concentrations (i.e., CO_2 and N_2O) during dynamic soil O_2.

While the spatial heterogeneity in soil O_2 loss may provide new understanding of hot spots, temporal heterogeneity in soil O_2 dynamics may be more important for determining hot moments. Short-term soil O_2 fluctuation was clearly linked to subsurface CO_2 and N_2O concentration dynamics. The simultaneous decrease in CO_2 and N_2O that we observed with big gulps (Figure 7d,e) suggests that soil gases are diffusion limited during saturation and soil drainage lifts this limitation. When diffusion constraints were removed, we also observed an increase in surface CO_2 flux that co-occurs with big gulps (Figure 7a). This result supports that the timing of big gulps may play an important role in increased soil-atmospheric gas exchange (hot moments). Change in surface N_2O and CH_4 fluxes were not significantly related to short-term soil O_2 dynamics perhaps due to the weaker subsurface response of N_2O concentration and no response of CH_4

concentration during dynamic soil O_2 (Figure 7e,f). Since soils were never completely anaerobic in our study, the availability of O_2 may have limited the production of N_2O and CH_4 under short-term saturation.

The timing and magnitude of big gulps are associated with soil drainage patterns (e.g, QD vs. SD saturation duration) driven by differences in soil properties such as soil texture and bulk density (Table 1). Furthermore, big gulps occur at a relatively consistent value of soil moisture near field capacity when soils begin to drain (Loecke et al. [in review]). This suggests that hot moments may depend on site-specific soil moisture patterns that correlate to big gulps. Others predict peak N_2O fluxes when soils are near field capacity due to the abundance of anaerobic microsites and increased diffusivity in the bulk soil (Davidson et al. 2000). In addition, field capacity at which max N_2O flux occurs depends on differences in soil properties that influence soil drainage patterns (i.e., total porosity and bulk density) (Castellano et al. 2010). Therefore, determining the soil physical properties that influence the magnitude and timing of big gulps may also reveal the abiotic factors that control the magnitude and timing of hot moments.

Surface GHG flux is a balance between the biogeochemical production/consumption of GHG and the transport of soil gases (Blagodatsky & Smith, 2012). Many studies describe increased soil gas flux rates due to soil re-wetting when low GHG surface flux from dry soils preceded rewetting events (Kim et al. 2012). Previous studies, however, lack mechanistic understanding of the environmental drivers of the microbial-mediated process rates, position of reactions sites, and physical transport of gases in the soil profile. With technical advancement and increased wide-spread use of

soil sensor networks, soil O_2 dynamics show greater potential for gleaning new information on coupled biogeochemical and soil physical processes under varying soil hydrology.

Soil O_2 dynamics are reported across multiple ecosystem (Burgin and Groffman 2012, Liptzen et al. 2010, Silver et al. 2012); yet, drivers of soil O_2 fluctuation are not well-represented in current ecosystem models that simulate soil O_2 directly from soil moisture (Loecke et al. [in review]). According to our study, soil O_2 dynamics can improve our mechanistic understanding of biogeochemical and physical shifts in the soil environment that influence hot spots and hot moments in GHG emission. The tight link between subsurface soil O_2 and CO_2 concentrations suggest that accurately modeling soil O_2 dynamics may further our capacity to predict rates of biogeochemical processes such as organic matter decomposition (Davidson et al. 2012). Additionally, near-continuous measurement of surface GHG fluxes may discern the time lag between subsurface GHG accumulation under soil O_2 depletion and short-term, enhanced rates of surface GHG fluxes under rapid soil gas transport. We recommend future efforts to collect soil GHG flux at higher temporal resolution following prolonged saturation (> 1 week) in order to highlight the influence of soil O_2 dynamics on biogeochemical hot moments.

References

Altor, A. E., & Mitsch, W. J. (2008). Pulsing hydrology, methane emissions and carbon dioxide fluxes in created marshes: A 2-year ecosystem study. *Wetlands*, *28*(2), 423–438.

Blagodatsky, S., & Smith, P. (2012). Soil physics meets soil biology: Towards better mechanistic prediction of greenhouse gas emissions from soil. *Soil Biology and Biochemistry*, *47*, 78–92.

Bodegom, P. M. Van, Leffelaar, P. A., Stams, A. J. M., & Wassmann, R. (1999). Modeling methane emissions from rice fields□: variability, uncertainty, and sensitivity analysis of processes involved, 1–18.

Burgin, A. J., Groffman, P. M., & Lewis, D. N. 2010. Factors Regulating Denitrification in a Riparian Wetland. *Soil Science Society of America Journal*, *74*(5), 1826.

Burgin, A. J., Yang, W. H., Hamilton, S. K., & Silver, W. L. 2011. Beyond carbon and nitrogen: how the microbial energy economy couples elemental cycles in diverse ecosystems. *Frontiers in Ecology and the Environment*, *9*(1), 44–52.

Burgin, A. J., & Groffman, P. M. 2012. Soil O_2 controls denitrification rates and N_2O yields in a riparian wetland. *Journal of Geophysical Research*, *117*(G1), G01010.

Castellano, M. J., Schmidt, J. P., Kaye, J. P., Walker, C., Graham, C. B., Lin, H., & Dell, C. J. (2010). Hydrological and biogeochemical controls on the timing and magnitude of nitrous oxide flux across an agricultural landscape. *Global Change Biology*, *16*(10), 2711–2720.

Chen, D., Li, Y., Grace, P., & Mosier, A. R. (2008). N_2O emissions from agricultural lands: a synthesis of simulation approaches. *Plant and Soil*, *309* (1-2), 169–189.

Clough, T. J., Sherlock, R. R., & Rolston, D. E. (2005). A review of the movement and fate of N_2O in the subsoil. *Nutrient Cycling in Agroecosystems*, *72*, 3–11. doi:10.1007/s10705-004-7349-z

Davidson, E. A., Keller, M., Erickson, H. E., Verchot, L. V., & Veldkamp, E. (2000). Testing a Conceptual Model of Soil Emissions of Nitrous and Nitric Oxides. *BioScience*, *50*(8), 667.

Davidson, E. A., Samanta, S., Caramori, S. S., & Savage, K. 2012. The Dual Arrhenius and Michaelis-Menten kinetics model for decomposition of soil organic matter at hourly to seasonal time scales. *Global Change Biology*, *18*(1), 371–384.

DeSutter, T. M., Sauer, T. J., & Parkin, T. B. (2006). Porous tubing for use in monitoring soil CO2 concentrations. *Soil Biology and Biochemistry*, *38*, 2676–2681.

Fierer, N., & Schimel, J. P. (2002). Effects of drying–rewetting frequency on soil carbon and nitrogen transformations. *Soil Biology and Biochemistry*, *34*(6), 777–787.

Fumoto, T., Kobayashi, K., Li, C., Yagi, K., & Hasegawa, T. (2007). Revising a process-based biogeochemistry model (DNDC) to simulate methane emission from rice paddy fieSDs under various residue management and fertilizer regimes. *Global Change Biology*, *14*(2), 382–402.

Groffman, P. M., Butterbach-Bahl, K., Fulweiler, R. W., Gold, A. J., Morse, J. L., Stander, E. K., Tague, C., Tonitto, C., & Vidon, P. (2009). Challenges to incorporating spatially and temporally explicit phenomena (hotspots and hot moments) in denitrification models. *Biogeochemistry*, *93*(1-2), 49–77.

Harris, R.: Effect of water potential on microbial growth and activity, in: Water potential relations in soil microbiology, edited by: Parr, J., Gardner, W., and Elliot, L., Soil Science Society of America, Madison, WI, USA, 23-97, 1981.

Hall, S. J., McDowell, W. H., & Silver, W. L. 2012. When Wet Gets Wetter: Decoupling of Moisture, Redox Biogeochemistry, and Greenhouse Gas Fluxes in a Humid Tropical Forest Soil. *Ecosystems*, *16*(4), 576–589.

Heinen, M. (2006). Simplified denitrification models: Overview and properties. *Geoderma*, *133*(3-4), 444–463.

Kim, D.-G., Vargas, R., Bond-Lamberty, B., & Turetsky, M. R. (2012). Effects of soil rewetting and thawing on soil gas fluxes: a review of current literature and suggestions for future research. *Biogeosciences*, *9*(7), 2459–2483.

Liptzin, D., Silver, W. L., & Detto, M. 2011. Temporal Dynamics in Soil Oxygen and Greenhouse Gases in Two Humid Tropical Forests. *Ecosystems*, *14*(2), 171–182.

McClain, M. E., Boyer, E. W., Dent, C. L., Gergel, S. E., Grimm, N. B., Groffman, P. M., … Pinay, G. (2003). Biogeochemical Hot Spots and Hot Moments at the Interface of Terrestrial and Aquatic Ecosystems. *Ecosystems*, *6*(4), 301–312.

Molodovskaya, M., Singurindy, O., Richards, B. K., Warland, J., Johnson, M. S., & Steenhuis, T. S. 2012. Temporal Variability of Nitrous Oxide from Fertilized Croplands: Hot Moment Analysis. *Soil Science Society of America Journal*, *76*(5), 1728.

NRC. 2001. Compensating for wetland losses under the Clean Water Act. National Academy Press, Washington, DC.

R Core Team. (2014). R: A language and environment for statistical computing. R Foundation for Statistical Computing, Vienna, Austria. ISBN 3-900051-07-0, URL http://www.R-project.org.

Riley, W. J., Subin, Z. M., Lawrence, D. M., Swenson, S. C., Torn, M. S., Meng, L., & Hess, P. 2011. Barriers to predicting changes in global terrestrial methane fluxes: analyses using CLM4Me, a methane biogeochemistry model integrated in CESM. *Biogeosciences*, *8*(7), 1925–1953.

Rubol, S., Manzoni, S., Bellin, A., & Porporato, A. (2013). Modeling soil moisture and oxygen effects on soil biogeochemical cycles including dissimilatory nitrate reduction to ammonium (DNRA). *Advances in Water Resources*, *62*, 106–124.

Ryals, R., & Silver, W. L. 2013. Effects of organic matter amendments on net primary productivity and greenhouse gas emissions in annual grasslands. *Ecological Applications : A Publication of the Ecological Society of America*, *23*(1), 46–59.

Sharifi, A., Kalin, L., Hantush, M. M., Isik, S., & Jordan, T. E. (2013). Carbon dynamics and export from flooded wetlands: A modeling approach. *Ecological Modelling*, *263*, 196–210.

Silver, W. L., Lugo, A. E., & Keller, M. 1999. Soil oxygen availability and biogeochemistry along rainfall and topographic gradients in upland wet tropical forest soils. *Biogeochemistry*, *44*(3), 301–328.

Silver, W. L., Liptzin, D., & Almaraz, M. 2012. Soil redox dynamics and biogeochemistry along a tropical elevation gradient. *Ecological Bulletins*, (54), 1–16.

Smith, K. A. S., All, T. B., Onen, F. C., Obbie, K. E. D., Assheder, J. M., & Ey, A. R. (2003). Exchange of greenhouse gases between soil and atmosphere : interactions of soil physical factors and biological processes. *European Journal of Soil Science*, (December), 779–791.

Mander, Ü., Maddison, M., Soosaar, K., & Karabelnik, K. (2011). The Impact of Pulsing Hydrology and Fluctuating Water Table on Greenhouse Gas Emissions from Constructed Wetlands. *Wetlands*, *31*(6), 1023–1032.

Teh, Y. A., Silver, W. L., & Conrad, M. E. (2005). Oxygen effects on methane production and oxidation in humid tropical forest soils. *Global Change Biology*, *11*(8), 1283–1297.

Vargas, R., Carbone, M. S., Reichstein, M., & Baldocchi, D. D. (2010). Frontiers and challenges in soil respiration research: from measurements to model-data integration. *Biogeochemistry*, *102*(1-3), 1–13.

West, A. W., & Sparling, G. P. (1986). Modifications to the substrate-induced respiration method to permit measurement of microbial biomass in soils of differing water contents. *Journal of Microbiological Methods*, *5*(3-4), 177–189.

Whalen, S. C. (2005). Biogeochemistry of methane exchange between natural wetlands and the atmosphere. *Environmental Engineering Science*, *22*(1).

Table Captions

Table 1. Average ± standard error for soil physical properties and substrate induced respiration at QD (n = 30) and SD (n = 18); *p<0.01 for QD and SD t test at 0-10 cm; ** p<0.01 for QD and SD t test at 0-10 cm and 10-20 cm. Average ± standard error for soil O_2 loss and saturation duration at QD 10 cm (n = 9 in 2013 and n = 24 in 2014), QD 20 cm (n = 7 in 2013 and n = 18 in 2014), SD 10 cm (n = 20 in 2014), and SD 20 cm (n = 15 in 2014).

Table 2. Percent of events in which CO_2, N_2O, and CH_4 concentration decreased following the big gulp and percent of events in which CO_2, N_2O, and CH4 surface flux increased following the big gulp; n = total number of big gulp events with GHG collected during saturation and within 24 hours following the big gulp.

Figure Captions

Figure 1. Distribution of percent sand at 0-10 cm from 120 soil cores collected across the post-construction wetland in 2011; site QD and SD were established in October 2013 and June 2014 and represent differences in soil texture at the wetland (a); the design of subsurface gas sampling chambers, soil sensors, and surface flux chamber for each soil pit at QD and SD (b).

Figure 2. Soil O_2 and soil moisture from June through August 2014 at SD "r1" 10 cm (a) and 20 cm (b).

Figure 3. Soil O_2 loss following June-August 2014 precipitation events at QD 10 cm (a), SD 10 cm (b), QD 20 cm (c), and SD 20 cm (d).

Figure 4. The relationship between saturation duration and the soil O_2 loss for QD and SD 10 cm (a) and 20 cm (b) following precipitation events in October 2013 and June-August 2014.

Figure 5. Subsurface CO_2, N_2O, and CH4, and O_2 concentration at QD "r1" 10 cm (a), SD "r1" 10 cm (b), QD "r1" 20 cm (c), and SD "r1" 20 cm (d).

Figure 6. Surface CO_2, N_2O, and CH4 fluxes and O_2 concentration at 10 cm at QD "r1" (a) and SD "r1" (b).

Figure 7. Change in surface CO_2 (a), N_2O (b), and CH_4 (c) flux and subsurface CO_2 (d), N_2O (e), and CH_4 (f) concentration (10 and 20 cm) as a function of change in soil O_2 concentration (*$p<0.05$) during October 2013 and from June-August 2014.

Tables

	QD 0-10 cm	QD 10-20 cm	SD 0-10 cm	SD 10-20 cm
Bulk Density ** ($g\ cm^{-3}$)	**1.26 ±** 0.05	**1.78 ±** 0.03	**1.40 ±** 0.03	**1.63 ±** 0.02
% Sand **	**52.76 ±** 3.61	**45.65 ±** 4.83	**22.61 ±** 0.57	**30.72 ±** 3.19
% Silt *	**24.36 ±** 3.52	**34.00 ±** 4.62	**52.96 ±** 0.56	**39.20 ±** 3.39
% Clay **	**22.87 ±** 0.45	**20.34 ±** 0.69	**24.42 ±** 0.54	**30.09 ±** 0.87
% Carbon	**2.21 ±** 0.12	**1.61 ±** 0.09	**2.18 ±** 0.07	**1.66 ±** 0.02
% Nitrogen **	**0.13 ±**0.006	**0.13 ±** 0.003	**0.21 ±** 0.004	**0.17 ±** 0.002
Substrate Induced Respiration * (CO_2 mg C g^{-1} soil hr^{-1})	**0.05 ±** 0.01	**0.04 ±** 0.004	**0.25 ±** 0.01	**0.06 ±** 0.01
	QD 10 cm	QD 20 cm	SD 10 cm	SD 20 cm
O_2 loss (%)	**4.29 ±** 1.57 (2013) **4.55 ±** 0.46 (2014)	**4.57 ±** 1.02 (2013) **4.36 ±** 0.57 (2014)	**5.77 ±** 0.93 (2014)	**6.59 ±** 1.13 (2014)
Saturation duration (days)	**0.8 ±** 0.13 (2014) **1.77 ±** 11.65 (2013)	**0.83 ±** 0.17 (2014) **4.11 ±** 1.17 (2013)	**1.04 ±** 0.13 (2014)	**2.54 ±** 0.46 (2014)

Table 1.

	CO_2	N_2O	CH_4
% increasing (mg m^{-2} hr^{-1} surface flux) n=16 (QD); n=13 (SD)	QD=63 SD=85	QD=13 SD=54	QD=31 SD=38
% decreasing (ppm_v at10 cm) n=16 (QD); n=13 (SD)	QD=50 SD=62	QD=63 SD=85	QD=44 SD=69
% decreasing (ppm_v at 20 cm) n=8 (QD); n=10 (SD)	QD=38 SD=90	QD=88 SD=100	QD=63 SD=50

Table 2.

Figures

a.

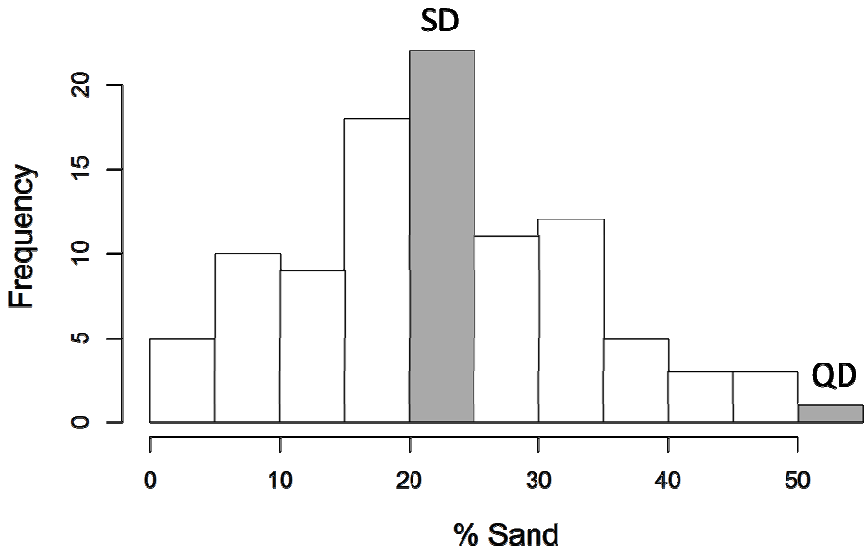

b.

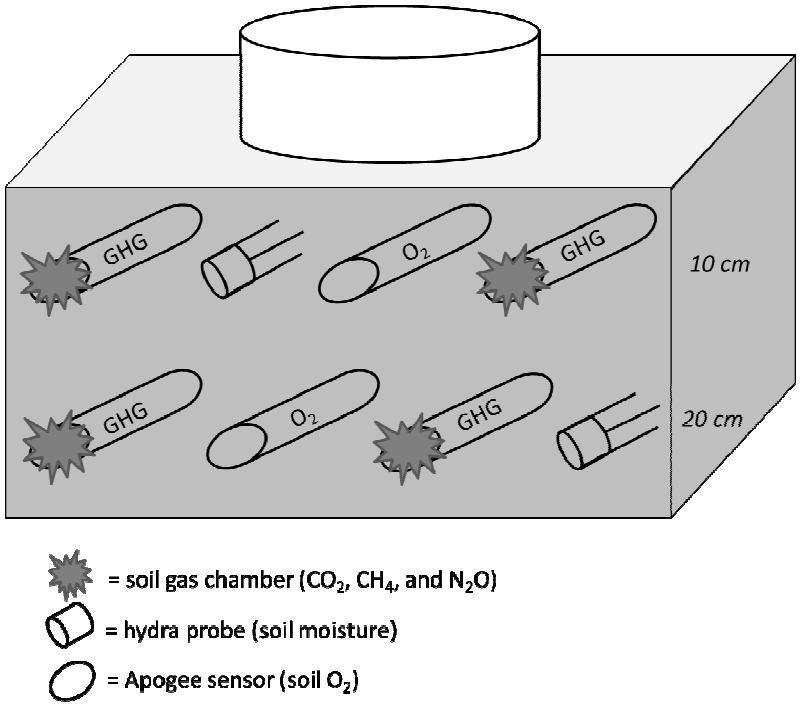

Figure 1.

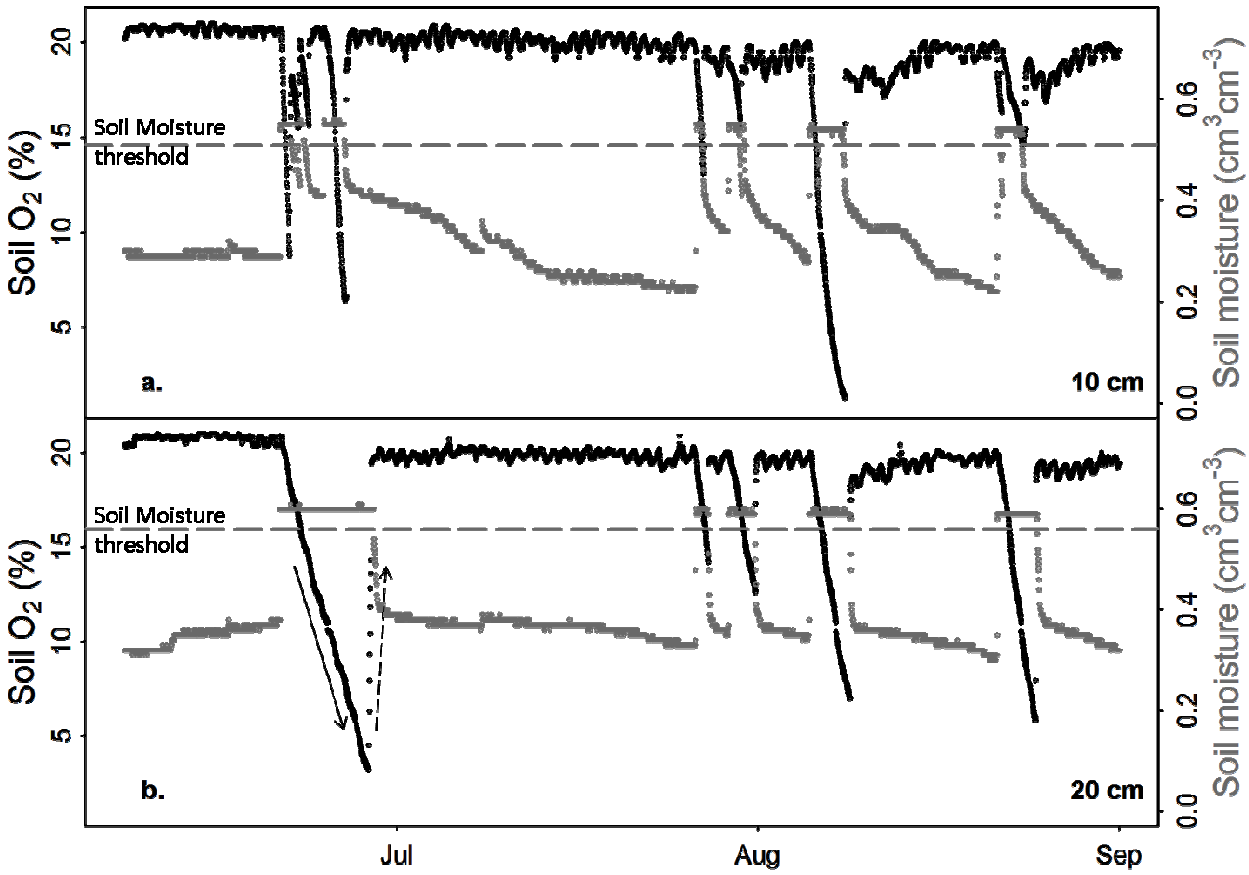
Soil O2 (%)
Soil Moisture threshold
a.
10 cm
Soil moisture (cm3cm-3)
Soil O2 (%)
Soil Moisture threshold
b.
20 cm
Soil moisture (cm3cm-3)
Jul
Aug
Sep

Figure 2.

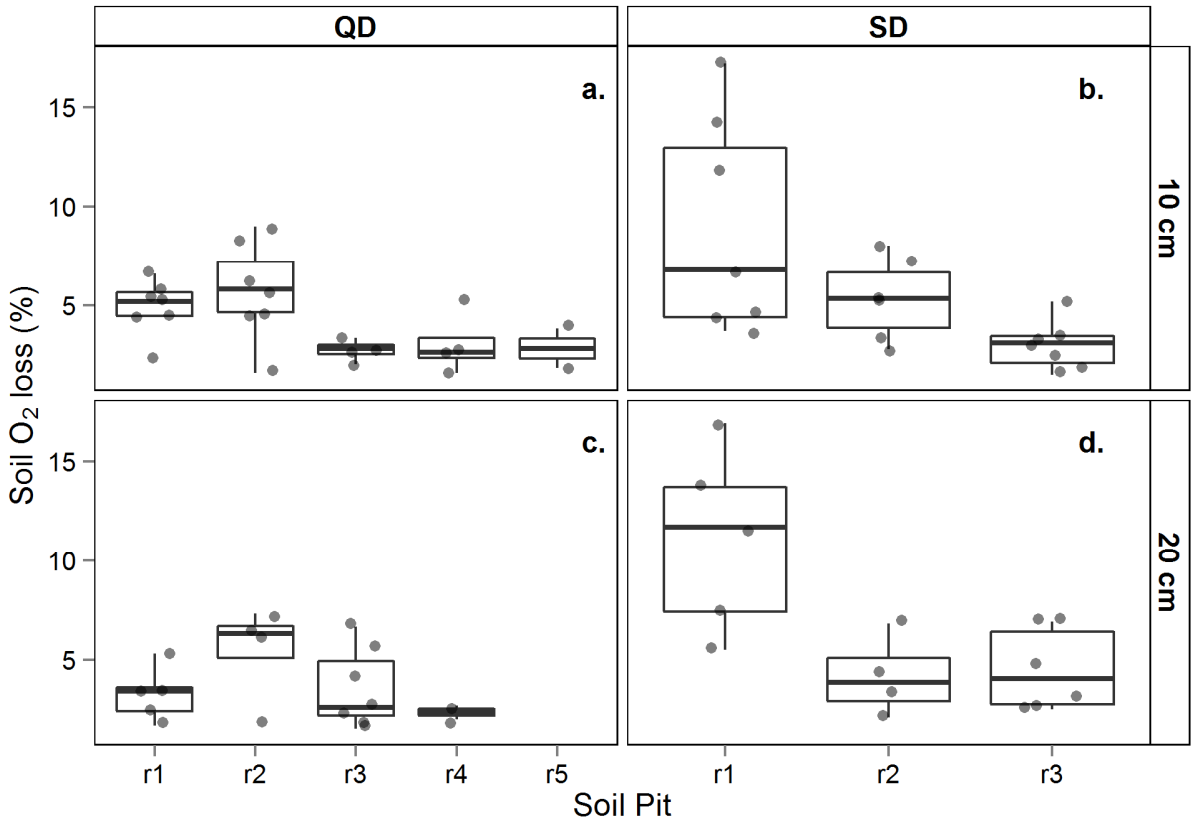

Figure 3.

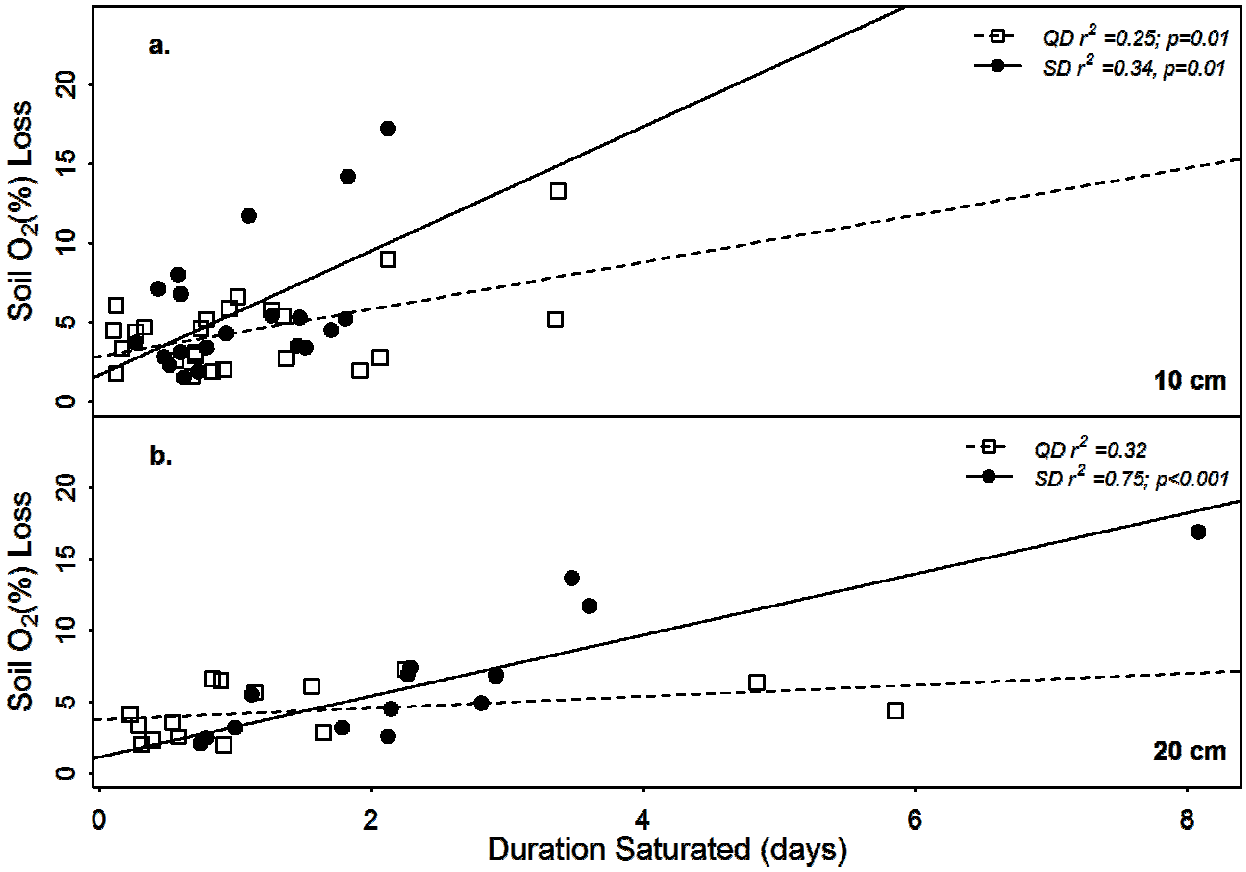
a.
QD r^2 =0.25; p=0.01
SD r^2 =0.34, p=0.01
10 cm
b.
QD r^2 =0.32
SD r^2 =0.75; p<0.001
20 cm
Soil O_2(%) Loss
Soil O_2(%) Loss
0
5
10
15
20
0
2
4
6
8
Duration Saturated (days)

Figure 4.

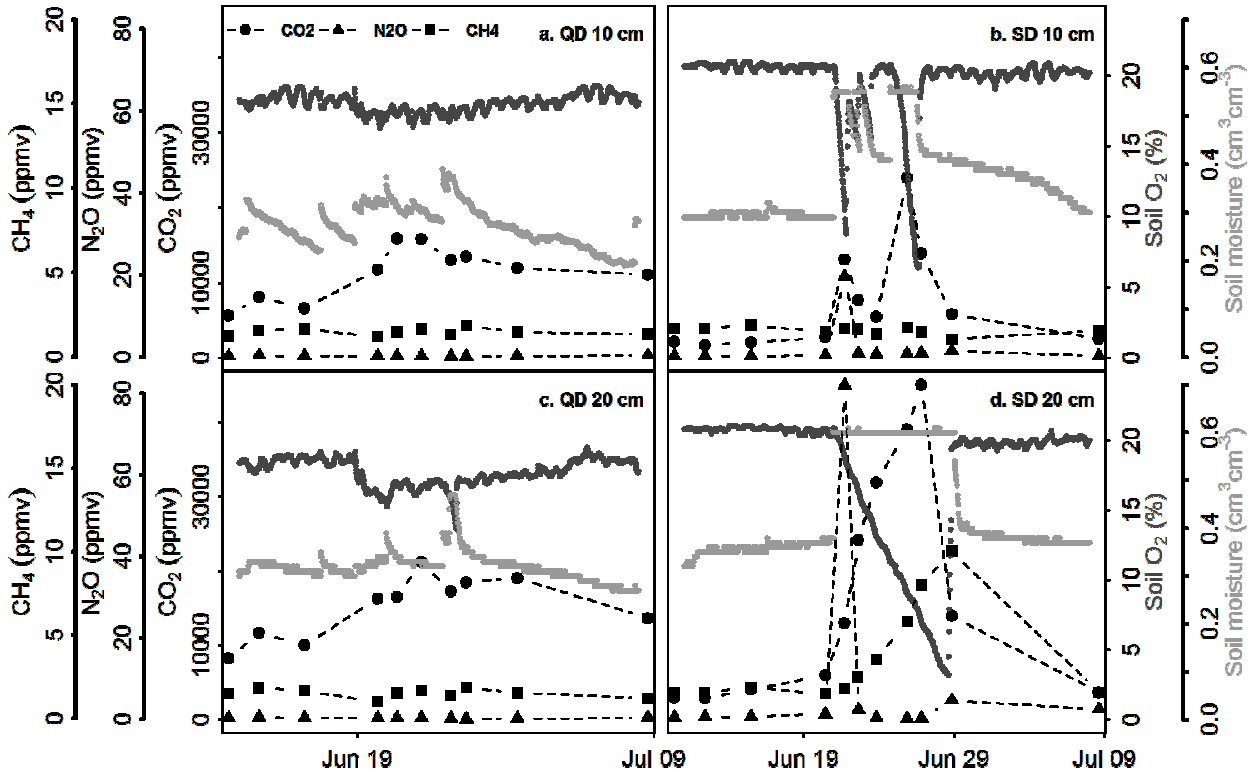
CO2
N2O
CH4
a. QD 10 cm
b. SD 10 cm
c. QD 20 cm
d. SD 20 cm
CH4 (ppmv)
N2O (ppmv)
CO2 (ppmv)
Soil O2 (%)
Soil moisture (cm3cm-3)
Jun 19
Jul 09
Jun 29

Figure 5.

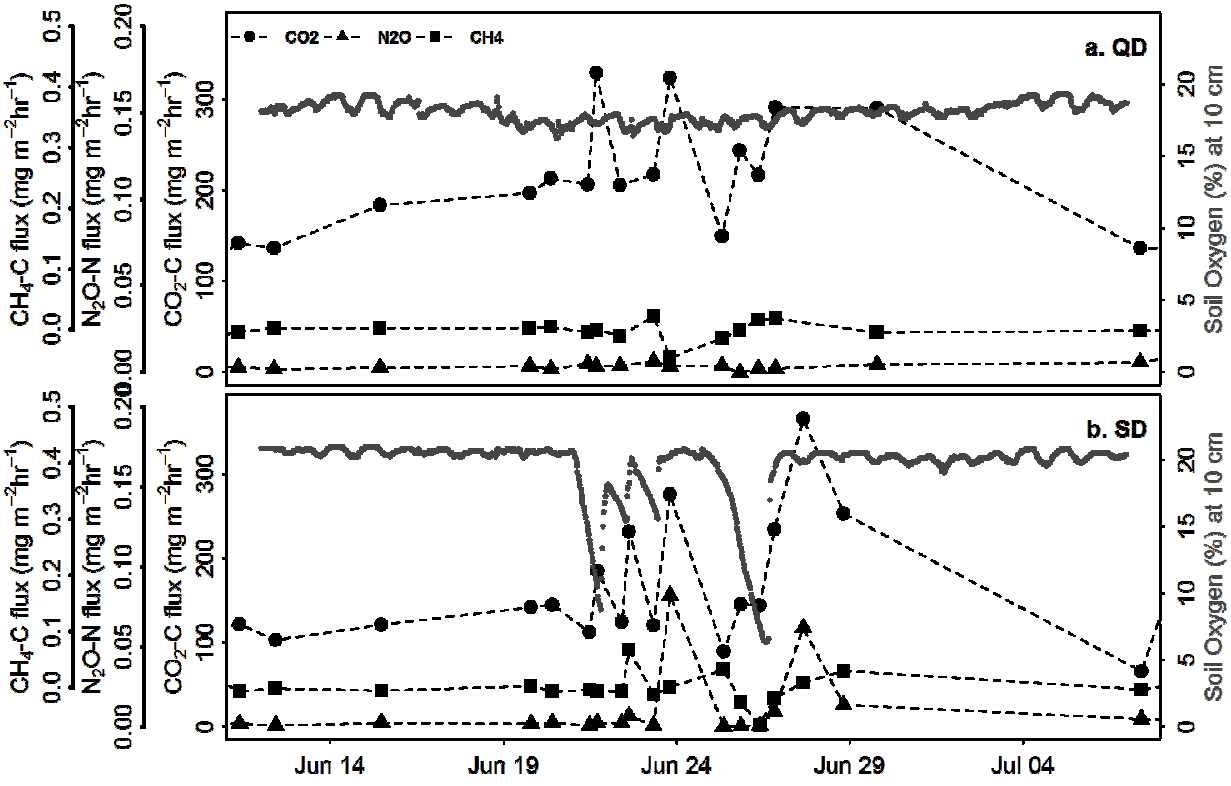
CO2
N2O
CH4
a. QD
b. SD
CH_4-C flux (mg $m^{-2}hr^{-1}$)
N_2O-N flux (mg $m^{-2}hr^{-1}$)
CO_2-C flux (mg $m^{-2}hr^{-1}$)
Soil Oxygen (%) at 10 cm
Jun 14
Jun 19
Jun 24
Jun 29
Jul 04

Figure 6.

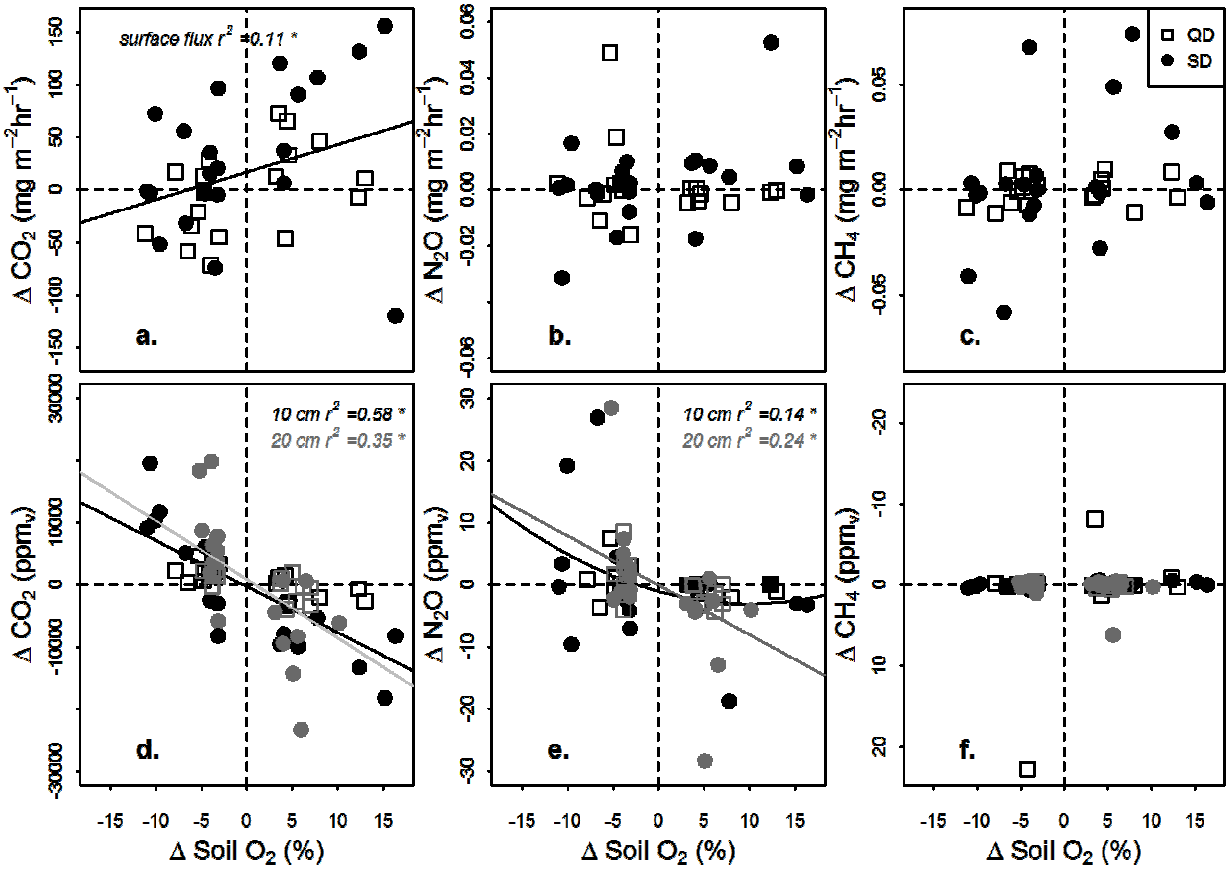
surface flux r² =0.11 *
10 cm r² =0.58 *
20 cm r² =0.35 *
10 cm r² =0.14 *
20 cm r² =0.24 *
QD
SD
a.
b.
c.
d.
e.
f.
Δ CO2 (mg m-2hr-1)
Δ N2O (mg m-2hr-1)
Δ CH4 (mg m-2hr-1)
Δ CO2 (ppmv)
Δ N2O (ppmv)
Δ CH4 (ppmv)
Δ Soil O2 (%)

Figure 7.